Direct Measurement Based $\mathcal{H}_\infty$ Controller Synthesis for an Autonomous Surface Vehicle

Gabriel Hugh Elkaim and Robert Kelbley
Autonomous Systems Lab, Computer Engineering, University of California at Santa Cruz

BIOGRAPHY

Gabriel Elkaim received the B.S. degree in Mechanical/Aerospace Engineering from Princeton University, Princeton NJ, in 1990, and both M.S. and Ph.D. Degrees from Stanford University, Stanford CA, in Aeronautics and Astronautics, in 1995 and 2002 respectively. In 2003, he joined the faculty of the Computer Engineering department, in the Jack Baskin School of Engineering, at the University of California, Santa Cruz, Santa Cruz CA, as an Assistant Professor. His research interests include control systems, sensor fusion, GPS, system identification, and autonomous vehicle systems. His research focuses on intelligent autonomous vehicles, with an emphasis on robust guidance, navigation, and control strategies. Specifically, he has founded the Autonomous Systems Lab at UC Santa Cruz, and is currently developing an autonomous wing-sailed marine surface vehicle and off-road autonomous ground vehicles.

Robert Kelbley is a graduate student at University of California, Santa Cruz. His research interests include group formation control and autonomous surface vehicles. Rob obtained a B.S. degree in Computer Engineering from Ohio Northern University, and is currently pursuing his Master's degree.

ABSTRACT

An autonomous surface vehicle, based on a Prindle-19 catamaran and substituting a self-trimming vertical wing for the sail, was developed to demonstrate precision guidance and control. This vehicle, the Atlantis, was demonstrated to track straight line segments to better than 0.3 meters $(1-\sigma)$ when already trimmed for sail along the segment, using LQG control based on an identified plant using the Observer Kalman Identification (OKID) methods. In this work, a way-point guidance system is tested experimentally in addition to a novel $\mathcal{H}_\infty$ subspace direct controller that is designed based on measured time series data for both the inputs and the actuator outputs. In previous simulations the Model Free Subspace $\mathcal{H}_\infty$ controller has demonstrated similar performance levels to LQG methods while using the same identification data, but without requiring a model structure. Results from experimental trials have proven less successful, motivating an analysis of the controller's implementation and possible problems.

INTRODUCTION

The Atlantis, an autonomous wind-propelled catamaran, has previously demonstrated an accuracy better than 0.3 meters $(1-\sigma)$ for line following applications when already trimmed for sail [2]. Atlantis' guidance and control architecture has since been extended allowing precision way-point guided marine navigation [3]. This paper continues previous research efforts in direct $\mathcal{H}_\infty$ control synthesis [3] and includes experimental validation of the segmented control as well as experimental results from the $\mathcal{H}_\infty$ direct control design. For completeness, the derivation of the $\mathcal{H}_\infty$ direct control is included.

The connection between system identification experiment design and the designer's control objectives must be taken into consideration when using experimental data in the control design process [6]. With this connection in mind, a direct control technique, "model free subspace $\mathcal{H}_\infty$ control" was applied to the Atlantis attempting to provide control design that was directly correlated to experimental system identification data in a model free fashion.

That is, normal system identification techniques require first building a mathematical model of the plant (hence the name: system identification). Using this model, a controller is designed and tested, and then the process is repeated until satisfactory performance is obtained. In a model free technique (often referred to as direct controller design), the controller is created directly from experimental data, avoiding an explicit model formation step. The model free subspace $\mathcal{H}_\infty$ control methodology utilizes subspace prediction methods directly coupled with $\mathcal{H}_\infty$ performance specifications.

The navigation guidance system demonstrated allows the Atlantis to perform precision, wind-propelled marine navigation where Autonomous Surface Vehicle (ASV) capabilities are required [11]. The key components of the Atlantis are discussed in the next section, including the realtime control system developed for segmented trajectory traversal. Next, an overview of model free subspace $\mathcal{H}_\infty$ control is presented. Experimental results for both PID and MFS$\mathcal{H}_\infty$ controllers are presented in the following section. A discussion of the failures of the $\mathcal{H}_\infty$ controller are highlighted next, and finally a conclusion is provided in the last section.

THE ATLANTIS

SYSTEM OVERVIEW

The Atlantis, pictured in Fig. 1, is an unmanned, autonomous, GPS-guided, wing-sailed sailboat. The Atlantis has demonstrated advanced precision control of a wind-propelled marine vehicle to an accuracy of better than one meter. The prototype is based on a modified Prindle-19 light catamaran.

Fig. 1. Atlantis with wing-sail, January 2001.

The wind-propulsion system is a rigid wing-sail mounted vertically on bearings to allow free rotation in azimuth about a stub-mast. Aerodynamic torque about the stub-mast is trimmed using a flying tail mounted on booms joined to the wing. This arrangement allows the wing-sail to automatically attain the optimum angle to the wind, and weather vane into gusts without inducing large heeling moments. Modern airfoil design allows for an increased lift to drag ratio (L/D) over a conventional sail, thus providing increased thrust while reducing the overturning moment.

The system architecture is based on distributed sensing and actuation, with a high-speed digital serial bus connecting the various modules together. Sensors are sampled at 100Hz., and a central guidance navigation and control (GNC) computer performs the estimation and control tasks at 5Hz. This bandwidth has been demonstrated to be capable of precise control of the catamaran.

The MIDG II Inertial Navigation System manufactured by Microrobics, Inc. provides position and attitude readings at a maximum of 50 Hz. This sensor system uses differential GPS (DGPS) for position and velocity measurements and includes a 3-axis rate gyro, 3-axis accelerometer, and 3-axis magnetometer.

PREVIOUS LINE FOLLOWING CONTROL RESULTS

In order to validate the performance of the controllers and all up system, closed loop control experiments were performed in Redwood City Harbor, California, on January 27, 2001. These tests were intended to verify that the closed loop controllers were capable of precise line following with the increased disturbances due to the wing-sail propulsion. System identification for the controller design was obtained previously using a trolling motor as the propulsion system, in place of the wing-sail which was still under construction. No modifications were made to the LQR controller design, and the tests were run on a day with approximately 10 knots (or 5 m/s) of wind, with gusts up to the 16 knot (or 8 m/s) range.

Upon analyzing the data, it was demonstrated that the Atlantis was capable of sailing to within 25 degrees of the true wind direction. Figure 2 presents a close-up of the first path of regulated control, and looks at the crosstrack error, azimuth error, and velocities while tracking a line. Note that the dark line in the top of the boat speed graph is the wind speed, and can be seen to vary well over 50% of nominal.

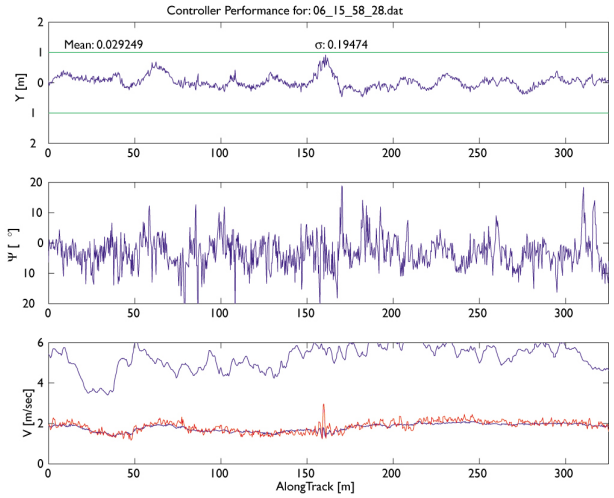

Fig. 2. Sailing path errors.

The mean of the crosstrack error is less than 3 cm., and the standard deviation is less than 30 cm., note that this is the Sailboat Technical Error (STE, the sailing analog of Flight Technical Error) defined as the difference between the position estimated by the GNC computer and the desired sailboat position. Previous characterization of the coast-guard differential GPS receiver indicated that the Navigation Sensor Error (NSE) is approximately 36 cm., thus the Total System Error (TSE) is less than 1 meter.

REALTIME CONTROL SYSTEM

The real time control system that generates trajectory and controller updates is implemented using an object oriented programming design, allowing a modular implementation for all sensor subsystems and actuator controllers. A set of interfaces was defined for each control subsystem, allowing the independent development of each module. This serialized approach allows the implementation of different rudder controllers without any changes to the central guidance system. For each sensor and actuator subsystem, a simulated module was also developed, providing Hardware-in-the-Loop testing capabilities from one central testing system. Fig. 3 provides a high level mapping of the major realtime control system objects.

To monitor system performance and update guidance system parameters after deployment from the dock, a graphical user interface (GUI) was developed to access all relevant

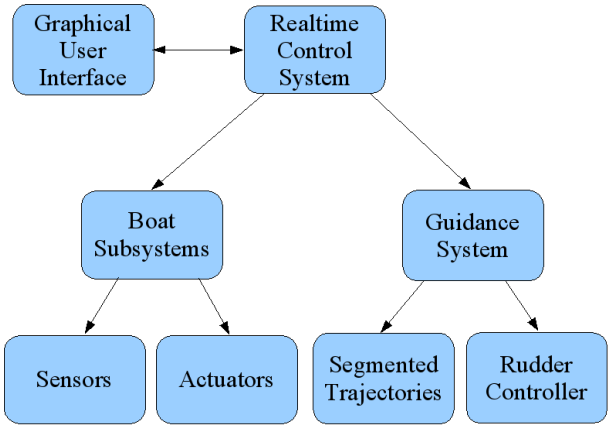

Fig. 3. Hierarchical layout of realtime control system.

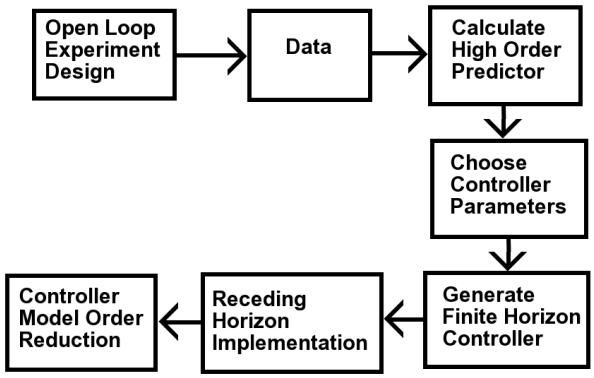

Fig. 4. Model free subspace $\mathcal{H}_\infty$ control design.

realtime control system variables. On-site access to the state and performance of each subsystem through the convenient windowed user interface provided quick verification and monitoring capabilities that was exploited throughout development and testing.

The programming language C♯ was used for the development of the different control system classes and GUI. Using C♯ provided accelerated development and debugging capabilities throughout the project, while also allowing existing C++ applications to be included within the same program.

MODEL FREE SUBSPACE $\mathcal{H}_\infty$ CONTROL

INTRODUCTION

Subspace system identification methods have recently become popular for the identification of linear time invariant (LTI) systems. Initially, experimental data is used to derive a least squares optimal predictor. The predictor can then be used to derive a state space model of the dynamic system. This derivation of the state space model from the predictor can be thought of as plant model order reduction. Instead of using this reduced order model for control design, model free control performs the control design directly from the subspace predictor, avoiding the formal model formation step in the design process.

Model free subspace $\mathcal{H}_\infty$ control exploits this subspace prediction method to provide a direct $\mathcal{H}_\infty$ control design technique. A single, integrated algorithm computes the $\mathcal{H}_\infty$-optimal controller and provides an estimate of the closed loop performance. For a more thorough discussion of subspace prediction and the model free subspace $\mathcal{H}_\infty$ controller see [15], [16].

Fig. 4 provides an overview of the model free subspace $\mathcal{H}_\infty$ control design procedure. Open loop experimental data is initially used to calculate a high order predictor. System performance specifications are defined using the weighting functions W_1 and W_2. The predictor and control parameters are then combined to form the controller.

The model free subspace based $\mathcal{H}_\infty$ control law utilizes a finite horizon cost function and is implemented with a "receding horizon" procedure. In this form, the control law is a member of a general class of controllers known as predictive control. Using a future horizon of length i, at the time k the optimal control u_{opt} is calculated. The control at time k is then implemented and data y_k and r_k are collected. The "horizon" is then shifted one step into the future and the procedure is repeated. The Atlantis uses a simple LTI discrete time system to express the receding horizon controller implementation. Standard model order reduction tools can then be applied to the LTI discrete time system if appropriate.

The reduction of the system identification step allows for an adaptive controller implementation that can adjust its performance specification as new closed loop input-output data is obtained. This adaptive implementation [17] will not be explored in this paper, although its existence offers substantial motivation for the application of these model free techniques.

As expected, the receding horizon controller implementation is derived from the $\mathcal{H}_\infty$ performance specification and the subspace predictor. The control design procedure can however, be viewed as a "black box" requiring the following steps:

1) Collect experimental data.
2) Select i,j, and weighting functions W_1,W_2.
3) Compute γ_{min} and reselect W_1,W_2 if necessary (ideally $\gamma_{min} \leq 1$). Finalize the choice of W_1, W_2 and choose $\gamma > \gamma_{min}$.
4) Compute and implement the final $i(m+l) + n_{w_1} + n_{w_2}$ order LTI control law and apply controller order reduction if necessary.

The following subsections outline the key elements of this novel control design technique. An in depth analysis of $\mathcal{H}_\infty$ control, including its advantages over $\mathcal{H}_2$ techniques, can be found in [8].

SUBSPACE PREDICTION

Consider data of length n from a MIMO plant where $u_k \in \mathbb{R}^m$ and $y_k \in \mathbb{R}^l$, m are the number of inputs, and l are the number of outputs. A subspace predictor can be generated from this data by choosing a specific prediction horizon, i, that is larger than the expected order of the LTI plant. This

prediction horizon is then used to break the data set into j prediction problems, where $j = n - 2i + 1$ and $j \gg i$. These j prediction problems are then used to generate the least squares optimal predictor $L_w \in \mathbb{R}^{il \times i(l+m)}$ and $L_u \in \mathbb{R}^{il \times im}$.

Using k as the present time index, we can then use L_w and L_u to predict future outputs given past experimental data and future inputs

$$\begin{bmatrix} \hat{y}_k \\ \vdots \\ \hat{y}_{k+i-1} \end{bmatrix} = L_w \begin{bmatrix} u_{k-i} \\ \vdots \\ u_{k-1} \\ y_{k-i} \\ \vdots \\ y_{k-1} \end{bmatrix} + L_u \begin{bmatrix} u_k \\ \vdots \\ u_{k+i-1} \end{bmatrix} \tag{1}$$

The derivation of L_w and L_u is reasonably straight forward. First, we define block Hankel matrices from the data using the subscript "p" to represent "past" data and "f" to represent the corresponding "future" data

$$U_p \triangleq \begin{bmatrix} u_0 & u_1 & \dots & u_{j-1} \\ u_1 & u_2 & \dots & u_j \\ \vdots & \vdots & \dots & \vdots \\ u_{i-1} & u_i & \dots & u_{i+j-2} \end{bmatrix} \in \mathbb{R}^{im \times j} \tag{2}$$

$$U_f \triangleq \begin{bmatrix} u_i & u_{i+1} & \dots & u_{i+j-1} \\ u_{i+1} & u_{i+2} & \dots & u_{i+j} \\ \vdots & \vdots & \dots & \vdots \\ u_{2i-1} & u_{2i} & \dots & u_{2i+j-2} \end{bmatrix} \in \mathbb{R}^{im \times j} \tag{3}$$

$$Y_p \triangleq \begin{bmatrix} y_0 & y_1 & \dots & y_{j-1} \\ y_1 & y_2 & \dots & y_j \\ \vdots & \vdots & \dots & \vdots \\ y_{i-1} & y_i & \dots & y_{i+j-2} \end{bmatrix} \in \mathbb{R}^{il \times j} \tag{4}$$

$$Y_f \triangleq \begin{bmatrix} y_i & y_{i+1} & \dots & y_{i+j-1} \\ y_{i+1} & y_{i+2} & \dots & y_{i+j} \\ \vdots & \vdots & \dots & \vdots \\ y_{2i-1} & y_{2i} & \dots & y_{2i+j-2} \end{bmatrix} \in \mathbb{R}^{il \times j} \tag{5}$$

All past data can then be combined as

$$W_p \triangleq \begin{bmatrix} U_p \\ Y_p \end{bmatrix} \tag{6}$$

Obtaining the best linear least squares predictor of Y_p given W_p and U_f can be formed as the Frobenius norm minimization

$$\min_{L_w, L_u} \left\| Y_f - \begin{bmatrix} L_w & L_u \end{bmatrix} \begin{bmatrix} W_p \\ U_f \end{bmatrix} \right\|_F^2 \tag{7}$$

The solution to this optimization problem is now given by the orthogonal projection of the row space of Y_f into the row space spanned by W_p and U_f. This orthogonal projection solution to (7) is given as

$$\hat{Y}_f = Y_f \Big/ \begin{bmatrix} W_p \\ U_f \end{bmatrix} \tag{8}$$

$$\triangleq Y_f \begin{bmatrix} W_p \\ U_f \end{bmatrix}^T \left(\begin{bmatrix} W_p \\ U_f \end{bmatrix} \begin{bmatrix} W_p \\ U_f \end{bmatrix}^T \right)^\dagger \begin{bmatrix} W_p \\ U_f \end{bmatrix} \tag{9}$$

where † denotes the Moore-Penrose or pseudoinverse. Therefore

$$\begin{bmatrix} L_w & L_u \end{bmatrix} = Y_f \begin{bmatrix} W_p \\ U_f \end{bmatrix}^T \left(\begin{bmatrix} W_p \\ U_f \end{bmatrix} \begin{bmatrix} W_p \\ U_f \end{bmatrix}^T \right)^\dagger \tag{10}$$

MODEL FREE SUBSPACE $\mathcal{H}_\infty$ CONTROL

The subspace predictor of the previous subsection will now be utilized to derive a finite-horizon, model free, subspace based, $\mathcal{H}_\infty$-optimal feedback controller. An $\mathcal{H}_\infty$ mixed sensitivity criteria is used to specify the desired minimum control performance and desired maximum control usage. Assuming a discrete time output unity feedback structure the specification used is

$$\left\| \begin{bmatrix} W_1 S \\ W_2 Q \end{bmatrix} \right\|_\infty \leq \gamma \tag{11}$$

where

$$S = (I + PK)^{-1} = G_{er} \tag{12}$$

$$Q = K(I + PK)^{-1} = G_{ur} \tag{13}$$

for some plant P and controller K, and W_1 and W_2 are weighting functions chosen to provide the desired system performance. Small S up to a desired cutoff frequency corresponds to each output tracking its reference well in the frequencies of interest. Limiting the magnitude of Q, especially at high frequencies, limits the control effort used.

The time-domain discrete-time expression for the specification in (11) is formulated as follows:

$$z \triangleq \begin{bmatrix} z_{w1} \\ z_{w2} \end{bmatrix} = \begin{bmatrix} w_1 * e \\ w_2 * u \end{bmatrix} = \begin{bmatrix} w_1 * (r - y) \\ w_2 * u \end{bmatrix} \tag{14}$$

where w_1 and w_2 are the respective discrete impulse responses of the discrete time weighting functions W_1 and W_2. Using (14), the finite-horizon problem of (11) can be written as

$$\sup_r J(\gamma) \leq 0, \text{ where } J(\gamma) = \sum_{t=0}^{i-1} (z_t^T z_t - \gamma^2 r_t^T r_t) \tag{15}$$

and the system is assumed to be at rest at $t = 0$. The length of the horizon, i, has been selected to be identical to the prediction horizon in the previous subsection, so (1) can be used to calculate $J(\gamma)$. Using $J(\gamma)$ from (15), the central finite-horizon $\mathcal{H}_\infty$ controller satisfies

$$\min_u \sup_r J(\gamma) \leq 0 \tag{16}$$

whenever the system is at rest at $t = 0$.

SUBSPACE BASED FINITE-HORIZON $\mathcal{H}_\infty$ CONTROL

Given the generalized plant of Fig. 5, the level-γ $\mathcal{H}_\infty$ control design problem is to choose a control u such that the finite-horizon $\mathcal{H}_\infty$ gain from r to z is of magnitude γ. This subsection derives the condition on γ that ensures that the problem is feasible, and computes the central solution for this $\mathcal{H}_\infty$ control problem.

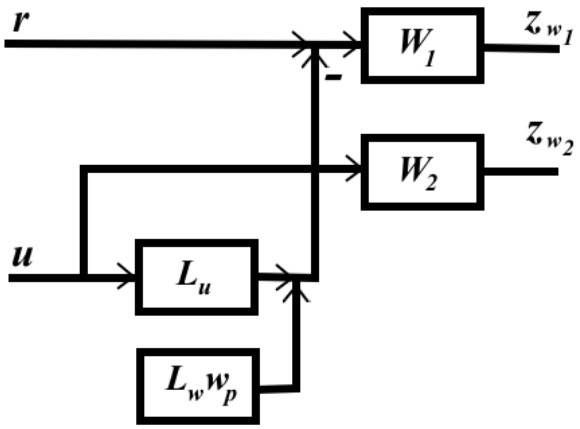

Fig. 5. Generalized plant for $\mathcal{H}_\infty$ control design.

If measurements of the plant input u, plant output y, and reference r are available for times $\{k-i,\ldots,k-2,k-1\}$, then the strictly causal, finite-horizon, model free, subspace based, level-γ, central $\mathcal{H}_\infty$ control for times $\{k,\ldots,k+i-1\}$ is

$$u_{opt} = -(L_u^T\tilde{Q}_1 L_u + Q_2)^{-1}\cdot \left[\begin{matrix}(L_u^T\tilde{Q}_1 L_w)^T \\ \left(-L_u^T(\gamma^{-2}\tilde{Q}_1 + I)H_1^T\Gamma_1\right)^T \\ (H_2^T\Gamma_2)^T\end{matrix}\right]^T \begin{bmatrix} w_p \\ x_{w_1} \\ x_{w_2}\end{bmatrix}_k \quad (17)$$

$$\tilde{Q}_1 = (Q_1^{-1} - \gamma^{-2}I)^{-1} \quad (18)$$

provided that

$$\gamma > \gamma_{min} \triangleq \sqrt{\overline{\lambda}[(Q_1^{-1} + L_u Q_2^{-1} L_u^T)^{-1}]} \quad (19)$$

where the discrete LTI weighting filters W_1 and W_2 have the minimal state space representation

$$(x_{w_1})_{k+1} = A_{w_1}(x_{w_1})_k + B_{w_1}(r_k - y_k) \quad (20)$$
$$(z_{w_1})_k = C_{w_1}(x_{w_1})_k + D_{w_1}(r_k - y_k) \quad (21)$$
$$(x_{w_2})_{k+1} = A_{w_2}(x_{w_2})_k + B_{w_2}(u_k) \quad (22)$$
$$(z_{w_2})_k = C_{w_2}(x_{w_2})_k + D_{w_2}(r_k - y_k) \quad (23)$$

The lower triangular Toeplitz matrices H_1 and H_2 are formed from the Markov parameters of the discrete weighting filters W_1 and W_2

$$H_1 \triangleq \begin{bmatrix} D_{w_1} & \ldots & 0 & \ldots & 0 \\ C_{w_1}B_{w_1} & \ldots & 0 & \ldots & 0 \\ C_{w_1}A_{w_1}B_{w_1} & \ldots & D_{w_1} & \ldots & 0 \\ \vdots & \vdots & \ddots & \vdots & \\ C_{w_1}A_{w_1}^{i-2}B_{w_1} & \ldots & C_{w_1}A_{w_1}^{i-4}B_{w_1} & \ldots & D_{w_1}\end{bmatrix} \quad (24)$$

$$H_2 \triangleq \begin{bmatrix} pD_{w_2} & \ldots & 0 & \ldots & 0 \\ C_{w_2}B_{w_2} & \ldots & 0 & \ldots & 0 \\ C_{w_2}A_{w_2}B_{w_2} & \ldots & D_{w_2} & \ldots & 0 \\ \vdots & \vdots & \ddots & \vdots & \\ C_{w_2}A_{w_2}^{i-2}B_{w_2} & \ldots & C_{w_2}A_{w_2}^{i-4}B_{w_2} & \ldots & D_{w_2}\end{bmatrix} \quad (25)$$

and

$$Q_1 \triangleq H_1^T H_1\ ,\ Q_2 \triangleq H_2^T H_2 \quad (26)$$

The extended observability matrices that contain the weighting filter impulse responses are defined as

$$\Gamma_1 \triangleq \begin{bmatrix} C_{w_1} \\ C_{w_1}A_{w_1} \\ \vdots \\ C_{w_1}A_{w_1}^{i-1}\end{bmatrix}\ ,\ \Gamma_2 \triangleq \begin{bmatrix} C_{w_2} \\ C_{w_2}A_{w_2} \\ \vdots \\ C_{w_2}A_{w_2}^{i-1}\end{bmatrix} \quad (27)$$

and vector of past plant inputs and outputs is defined as

$$(w_p)_k \triangleq \begin{bmatrix} u_{k-i} \\ \vdots \\ u_{k-1} \\ y_{k-i} \\ \vdots \\ y_{k-i}\end{bmatrix}. \quad (28)$$

MFS$\mathcal{H}_\infty$ PREDICTIVE CONTROL

The final step of the control design procedure, the receding horizon implementation, is expressed as the following MIMO LTI discrete time system :

$$\begin{bmatrix} u_p \\ y_p \\ x_{w_1} \\ x_{w_1} \end{bmatrix}_{k+1} = \begin{bmatrix} \begin{bmatrix} S_m \\ k_1 \end{bmatrix} & \begin{bmatrix} 0 \\ k_2 \end{bmatrix} & \begin{bmatrix} 0 \\ k_3 \end{bmatrix} & \begin{bmatrix} 0 \\ k_4 \end{bmatrix} \\ 0 & \begin{bmatrix} S_l \\ 0 \end{bmatrix} & 0 & 0 \\ 0 & 0 & A_{w_1} & 0 \\ B_{w_2}k_1 & B_{w_2}k_2 & B_{w_2}k_3 & A_{w_2} + B_{w_2}k_4 \end{bmatrix} \begin{bmatrix} u_p \\ y_p \\ x_{w_1} \\ x_{w_1} \end{bmatrix}_k + \begin{bmatrix} 0 & 0 \\ 0 & \begin{bmatrix} 0 \\ I_l \end{bmatrix} \\ B_{w_1} & B_{w_1} \\ 0 & 0 \end{bmatrix} \begin{bmatrix} r \\ y \end{bmatrix}_k \quad (29)$$

$$u_k = \begin{bmatrix} k_1 & k_2 & k_3 & k_4 \end{bmatrix} \begin{bmatrix} u_p \\ y_p \\ x_{w_1} \\ x_{w_2} \end{bmatrix}_k \quad (30)$$

where $u_k \in \mathbb{R}^m$, $r_k \in \mathbb{R}^l$, $y_k \in \mathbb{R}^l$, m are the number of plant inputs, and l are the number of plant outputs. I_m and I_l are defined as $m \times m$ and $l \times l$ identity matrices respectively,

$$S_m = \begin{bmatrix} 0 & I_m & 0 & \dots & 0 \\ 0 & 0 & I_m & \dots & 0 \\ \vdots & \vdots & \vdots & \ddots & 0 \\ 0 & 0 & 0 & \dots & I_m \end{bmatrix} \in \mathbb{R}^{(i-1)m \times im} \quad (31)$$

$$S_l = \begin{bmatrix} 0 & I_l & 0 & \dots & 0 \\ 0 & 0 & I_l & \dots & 0 \\ \vdots & \vdots & \vdots & \ddots & 0 \\ 0 & 0 & 0 & \dots & I_l \end{bmatrix} \in \mathbb{R}^{(i-1)l \times il} \quad (32)$$

and

$$\begin{bmatrix} k_1 & k_2 \end{bmatrix} = \left\{ -(L_u^T \tilde{Q}_1 L_u + Q_2)^{-1} L_u^T \tilde{Q}_1 L_w \right\}_{1:m,:} \quad (33)$$

$$k_3 = \left\{ (L_u^T \tilde{Q}_1 L_u + Q_2)^{-1} L_u^T (\gamma^{-2} \tilde{Q}_1 + I) H_1^T \Gamma_1 \right\}_{1:m,:} \quad (34)$$

$$k_4 = \left\{ -(L_u^T \tilde{Q}_1 L_u + Q_2)^{-1} H_2^T \Gamma_2 \right\}_{1:m,:} \quad (35)$$

where $\{\bullet\}_{1:m,:}$ means extract the first m rows of the matrix $\bullet$, and $k_1 \in \mathbb{R}^{m \times im}$, $k_2 \in \mathbb{R}^{m \times il}$, $k_3 \in \mathbb{R}^{m \times n_{w_1}}$, $k_4 \in \mathbb{R}^{m \times n_{w_2}}$.

EXPERIMENTAL SETUP

A series of experimental trials were run from August 31 through September 18, 2006 at the Santa Cruz harbor, testing the extensions to Atlantis' guidance and control system previously developed in [3] and [1]. The full wing sail propulsion unit was substituted with an electric trolling motor in this initial testing phase, with the assumption that guidance and control system performance should be independent of the propulsion unit used.

Initial testing was performed to validate the segmented trajectory guidance system specified in [3]. A PID controller was used to track line and arc segments inside the Santa Cruz harbor and fully test the integration of the real time control system with sensor and actuator subsystems. Further testing focused on the implementation of the model free subspace $\mathcal{H}_\infty$ controller developed in [1].

PID RESULTS

The Atlantis' guidance system uses a series of GPS way-points for input, and then transforms those way-points into a series of line segments connected by arcs of a constant radius as trajectories for navigation. This way-point guidance system can be used by any way-point planning algorithm, and future work will focus on the implementation of algorithms designed for obstacle avoidance and optimal navigation through flows.

On August 31, 2006 a PID controller was used to monitor heading errors (Ψ) and crosstrack deviations (Y). The exact gains developed in simulations [3] were used and provided excellent results for traversal along interconnected line and arc segments within the harbor. Figures 6 and 7 show the path and attitude of the Atlantis for a given set of way-points and the corresponding error signals for that path. Notice that initially a drive-to-line controller was used to lock on to the first segment. After acquisition of the first line segment, the mean crosstrack error for the segments was 0.08 meters with a standard deviation of 0.21 meters.

MODEL FREE SUBSPACE $\mathcal{H}_\infty$ RESULTS

In addition to the stable performance exhibited by PID control, previous simulation work has shown that different linear optimal control techniques, specifically model free subspace $\mathcal{H}_\infty$ control, can provide a significant improvement in performance, especially in the presence of unknown wind and water disturbances. Unfortunately, extensive testing of these MFS$\mathcal{H}_\infty$ techniques in the field were unsuccessful. Multiple factors most likely hindered this direct control design technique, which will be discussed in the following section. This section will outline one set of controller parameters used during experimental testing.

As discussed in the Subspace Prediction subsection, the subspace predictor is generated using experimental input-output data of length n. A prediction horizon, i, is then chosen that breaks the data set into j prediction problems, where $j = n - 2i + 1$. To ensure an accurate predictor is created for a LTI model, i was chosen to be at least twice as large the expected plant order.

Multiple system identification trials were performed to gather open-loop system identification data. The data used to generate the subspace predictor is shown in Fig. 8. The boat uses rudder slew rate ($\dot{\delta}$) as the input signal and has three output signals: cross-track (Y), azimuth (Ψ), and effective rudder angle (δ).

Although the Atlantis is a nonlinear system, the first section outlines how LQG techniques are effective for precision control when small azimuth and cross-track deviations are

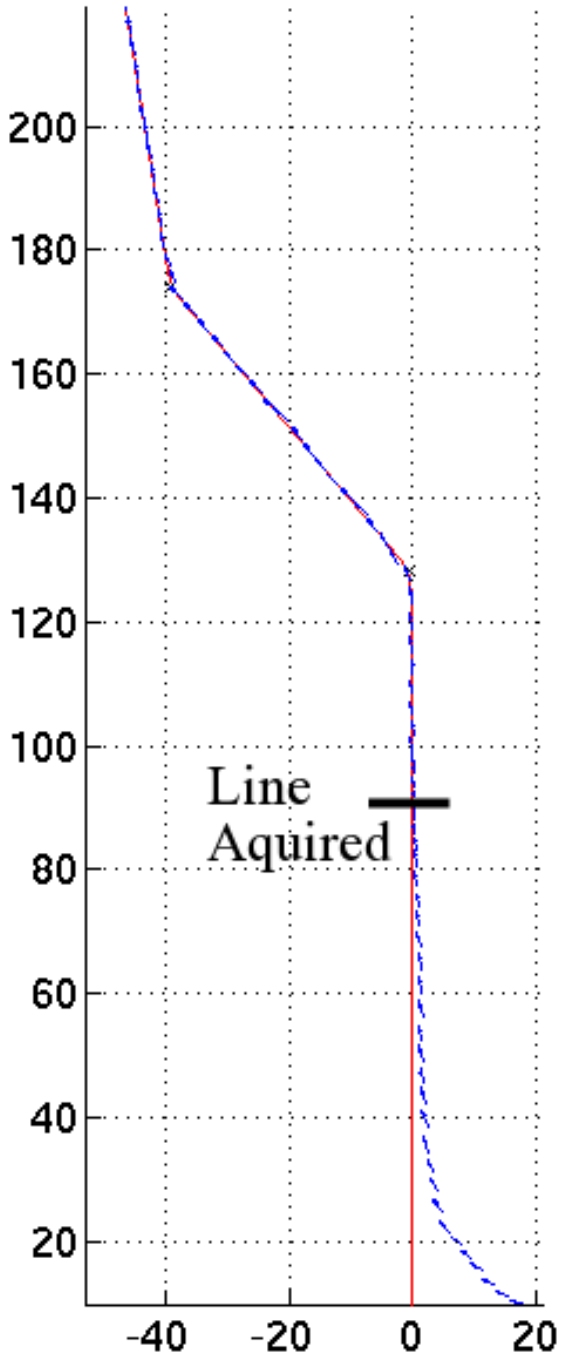

Fig. 6. Segmented trajectories (red) and boat position and attitude (blue). Axes in meters.

maintained. A variety of predictors were generated at different orders and verified with various system identification data trials. The best prediction horizon was obtained by choosing a predictor with $i = 20$. Fig. 9 shows the predictor performs very well at predicting rudder angle (δ), however provided a poor prediction in the crosstrack (Y) and heading error (Ψ).

For comparison, reconstruction of previous simulated work is plotted in Fig. 10.

As shown in the Model Free Subspace $\mathcal{H}_\infty$ Control

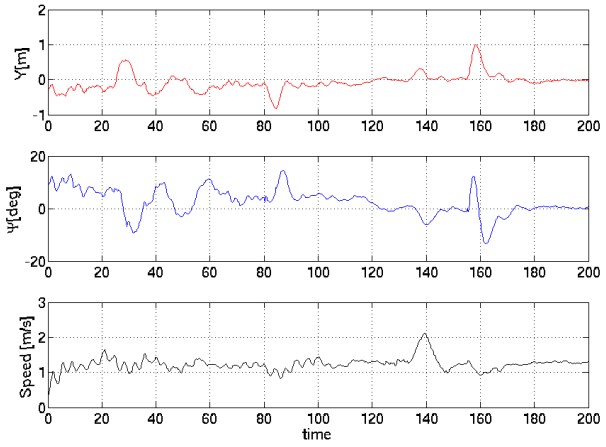

Fig. 7. Errors from segmented trajectory traversal.

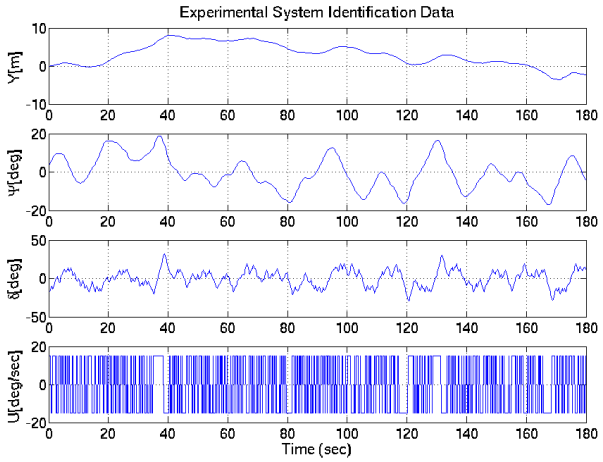

Fig. 8. System identification data created by controlling the slew rate of the Atlantis with a pseudo-random binary sequence stabilized around predefined heading and rudder angle limits.

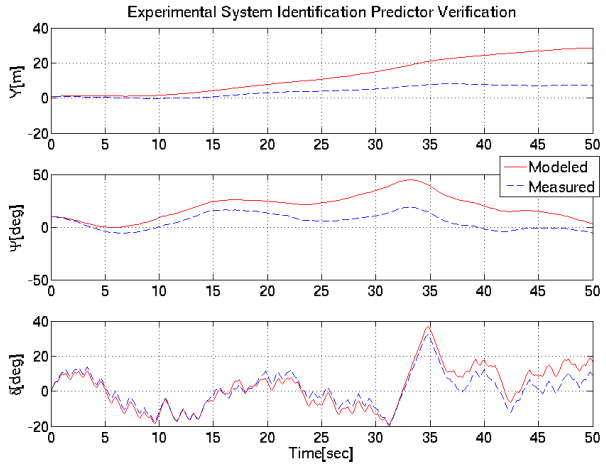

Fig. 9. The subspace predictor reconstruction of an experimental system identification pass comparing measured outputs to predicted values.

subsection, W_1 and W_2 are weighting functions chosen to provide the desired system performance for the mixed

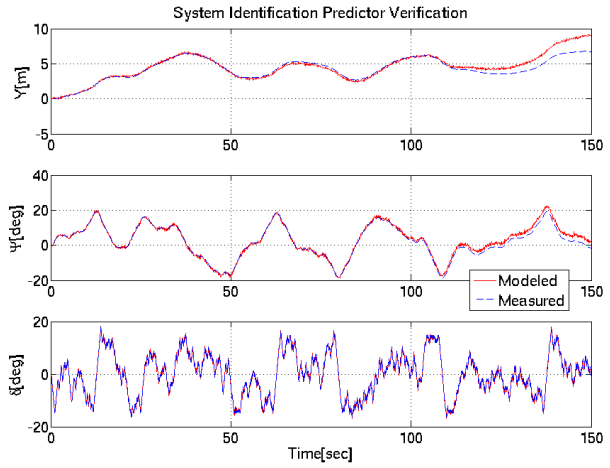

Fig. 10. A subspace predictor reconstruction of a simulated system identification pass comparing measured outputs to predicted values.

sensitivity criteria given in (11). It is important to note that increasing either the DC gain or bandwidth of W_1 will make the controller more aggressive. This will force the controller to track higher error signal frequencies making the response faster, but less damped. Decreasing W_2 will permit greater control usage, which is typically not desirable at high frequencies. However, if W_1 is increased, requesting higher performance, but W_2 is not sufficiently decreased, to provide more control usage, the problem will become over constrained. These over lapping constraints will be reflected by γ_{opt} increasing over the nominal value of one. W_1 and W_2 were then selected with these performance tradeoffs in mind.

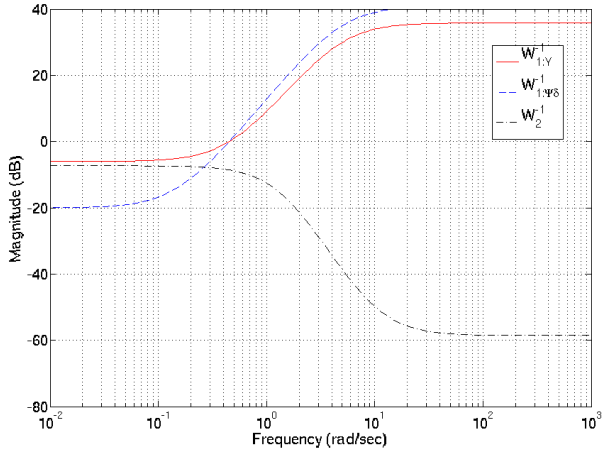

Fig. 11. Sample control specification used.

Fig. 11 shows the inverse of each weighting function chosen for one of the more successful experimental controller tests. Identical W_1 functions were used to specify the performance requirements for Ψ, and δ. As shown, the design cutoff frequency is around 0.35 rad/sec (20 Hz). It is desirable that all three outputs stay nominally around zero to provide a more linear response of the system, therefore 6 dB of rejection at DC was chosen for Y and 20 dB of rejection at DC was chosen for Ψ and δ. The control usage function, W_2, which effects the slew rate of the rudders was then selected to penalize control usage at higher frequencies.

Variations of the previous controller parameters were used to generate multiple MFS$\mathcal{H}_\infty$ controllers. Performance varied from severe underdamping resulting in large overshoots, to control instability. Fig. 12 and 13 show the results of one poorly damped trial run. Although weighting filter values were varied, an acceptable controller was not obtained.

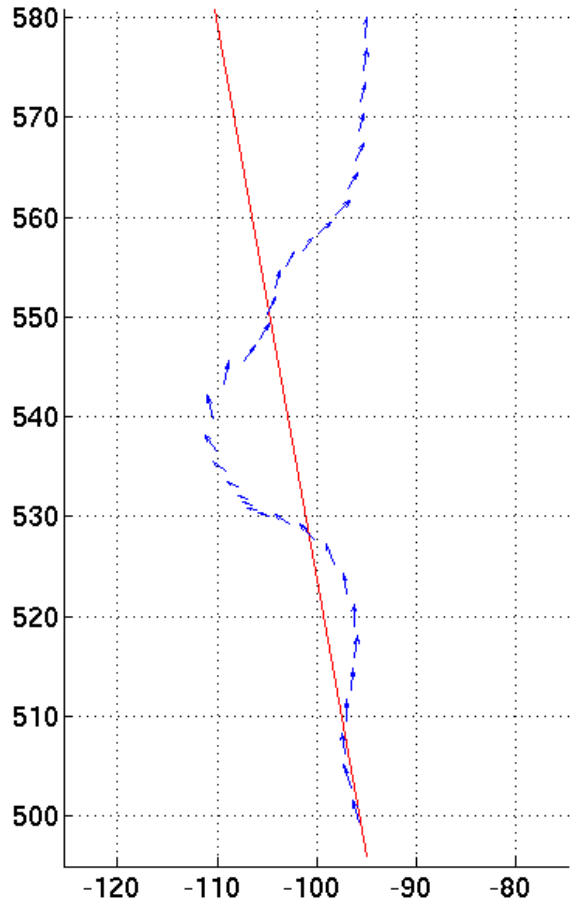

Fig. 12. Segmented trajectories (red) and boat position and attitude (blue). Note boat eventually looses stability and switched to manual control. Axes in meters.

MFS$\mathcal{H}_\infty$ FAILURE ANALYSIS

A detailed analysis of the model free subspace $\mathcal{H}_\infty$ controller field test data suggests that multiple problems may have compromised the performance of this direct control technique. This subsection will look at several issues, and provide suggestions for various adjustments to overcome these issues.

As shown in Fig. 8, the predictor did not function nearly as well as it had in comparable catamaran simulations, showing a breakdown after approximately 4 seconds (whereas simulations showed acceptable performance for over 100

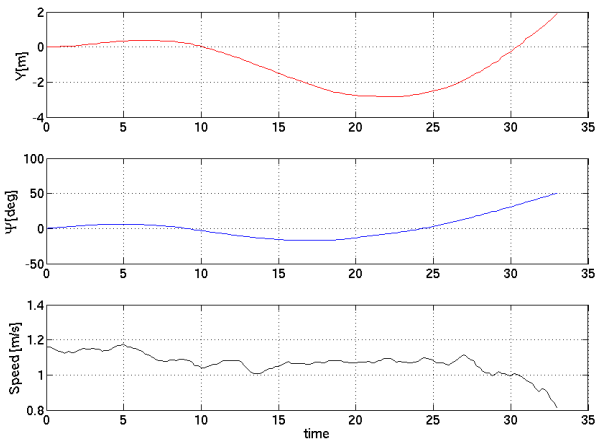

Fig. 13. Errors from segmented trajectory traversal.

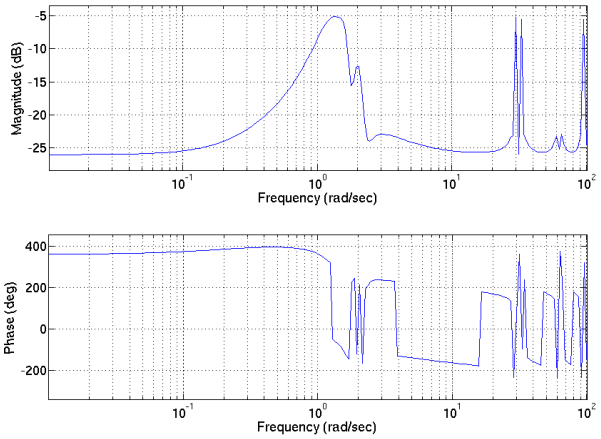

Fig. 14. Bode plot of MFS$\mathcal{H}_\infty$ controller used in experimental trials.

seconds). Previous studies had shown that the direct control $\mathcal{H}_\infty$ design is very sensitive to nonlinearities in the system. In our current system identification passes, the rudder slew rate was changed every 200 msec, which exacerbated the nonlinearities in the actuator system (compliance in the gear/chain, backlash in the shaft coupling, etc.). Furthermore, the rapid changes in rudder angle keep the boat in a very nonlinear region before the forces have time to stabilize and set, allowing a steady state rotation rate of the hulls.

We contrast this with the previous system identification efforts, which used a human to drive the input slew rate to the system. With this technique, the slew rate was varied much slower, and the heading rate allowed to reach steady state before the next input was injected. The high frequency chatter on the rudder slew rate imposed by the computer control is felt to have pulled the response out of the linear region, and thus caused the predictor to fail.

One important element of $\mathcal{H}_\infty$ controllers is that they are frequency agnostic, meaning they will increase controller bandwidth as high as possible if better performance can be obtained in these higher frequencies. The bode plot showing the frequency response of $\frac{\delta(j\omega)}{Y(j\omega)}$ for one controller is provided in Fig. 14. Although weighting filters were used to penalize performance and control usage at higher frequencies, the MFS$\mathcal{H}_\infty$ controller shows a propensity for high frequency excitation, which is not desirable for systems with tight linearization constraints.

CONCLUSIONS

A control architecture for an autonomous sailboat using a way-point navigation system has been tested, including a model free subspace $\mathcal{H}_\infty$ controller. This guidance system is capable of precision way-point navigation to an accuracy of better than 0.35 meters $(1-\sigma)$ under PID control. Although the MFS$\mathcal{H}_\infty$ demonstrated very impressive trajectory following performance in previous simulations, its implementation left much to be desired. It is felt that the driving frequency of the injected input was too high, and forced the system out of the linear realm, while at the same time, the weighting functions for control design may be less than optimal. While the $\mathcal{H}_\infty$ techniques are part of the robust control family, they remain very sensitive to nonlinearities, which can destroy their performance very quickly.

Other future work will include a way-point generation methodology that will avoid stationary obstacles and also optimally determine trajectories given only a destination point and weather data forecasts to predict future wind and wave activity. This added navigation system combined with will create a wind-propelled ASV capable of robust navigation.

REFERENCES

[1] G. Elkaim, B. Woodley, and R. Kelbley. Model free subspace control for an autonomous catamaran. *IEEE/ION PLANS Conference*, 2006.

[2] G.H. Elkaim. *System Identification for Precision Control of a Wing-sailed GPS-Guided Catamarn*. PhD thesis, Stanford University, 2001.

[3] G.H. Elkaim and R.J. Kelbley. Control architecture for segmented trajectory following of a wind-propelled autonomous catamaran. *AIAA Guidance, Navigation, and Control Conference*, August 2006.

[4] P. Encarnacao, A. Pascoal, and M. Arcak. Path following for autonomous marine craft. *5th IFAC Conference on Maneuvering and Control of Marine Craft*, pages 117–22, 2000.

[5] T.I. Fossen. *Guidance and Control of Ocean Vehicles*. Wiley and Sons, New York, NY, 1994.

[6] M. Gevers. Identification for control: From the early achievements to the revival of experiment design. *European Journal of Control*, 11:335–352, 2005.

[7] J.-N. Juang. *Applied System Identification*. Prentice Hall, NJ, 1994.

[8] K.Zhou. *Robust and Optimal Control*. Prentice-Hall, Inc., Upper Saddle River, NJ, 1996.

[9] E. Lefeber, KY. Pettersen, and H. Nijmeijer. Tracking control of an underactuated ship. *IEEE Transactions on Control Systems Technology*, 3:52–61, January 2003.

[10] B.W. McCormick. *Aerodynamics, Aeronautics, and Flight Mechanics*. John Wiley and Sons, New York, NY, 1979.

[11] A. Pascoal, P. Olivera, and C. Silvestre. Robotic ocean vehicles for marine science applications: The european asimov project. *OCEANS 2000 MTS/IEEE Conference and Exhibition*, 1:409–415, 2000.

[12] R.S.Shevell. *Fundamentals of Flight*. Prentice-Hall, Inc., Englewood Cliffs, NJ, 1983.

[13] R. Skjetne and T. Fossen. Nonlinear maneuvering and control of ships. *MTS/IEEE OCEANS 2001*, 3:1808–15, 2001.

[14] T. VanZwieten. *Dynamic Simulation and Control of an Autonomous Surface Vehicle*. PhD thesis, Florida Atlantic University, 2003.

[15] B.R. Woodley. *Model Free Subspace Based $\mathcal{H}_\infty$ Control*. PhD thesis, Stanford University, 2001.

[16] B.R. Woodley, J.P. How, and R.L. Kosut. Model free subspace based $\mathcal{H}_\infty$ control. *Proceedings of the American Control Conference*, pages 2712–2717, 2001.

[17] B.R. Woodley, J.P. How, and R.L. Kosut. Subspace based direct adaptive $\mathcal{H}_\infty$ control. *Int. J. Adapt. Control Signal Process*, 15:535–561, 2001.